Available online at www.sciencedirect.com

SciVerse ScienceDirect

Procedia CIRP 8 (2013) 45 – 50

www.elsevier.com/locate/procedia

14th CIRP Conference on Modeling of Machining Operations (CIRP CMMO)

Simulation of Distortion due to Machining of Thin-walled Components

V. Schulze[a], P. Arrazola[b], F. Zanger[a], J. Osterried[a,*]

[a] *Karlsruhe Institute of Technology (KIT), wbk Institute of Production Science, Kaiserstaße 12, 76131 Karlsruhe, Germany*
[b] *Mondragon University, Mechanical and Manufacturing Department, Loramendi, 4, 20500 Arrasate-Mondragón, Spain*
* Corresponding author. Tel.: +49 721 608-46316; fax: +49 721 608-45004 . *E-mail address*: julius.osterried@kit.edu.

Abstract

The distortion of components is strongly related to the residual stress state induced by manufacturing processes like heat treatment, forming or machining. Each process step affects the initial stress state of the following process step. When removing material during machining, the component establishes a new stress equilibrium. Stresses are redistributed causing the component geometry to adjust. Especially for thin-walled components distortion potential is high. Gaining knowledge about the influence of initial loads and the release of distortion during machining processes helps to increase product quality and efficiency. The influences of different initial stress states and different machining parameters on the amount of distortion are examined using both FEM simulations and experiments. A thin-walled T-profile made of aluminum alloy Al 7075-T6 serves as test specimen. A bending process applies a load to initialize a repeatable and defined residual stress state. A groove was machined afterwards into the plastically deformed work piece to trigger stress redistribution and a release of distortion. Different loads with 35 to 45 kN and two different geometries of a groove were used. The amount of initial stress has a significant effect on the distortion potential which could be quantified in the study. Simulations show the same behavior as the experiments and the results match very well especially for a high load.

Selection and peer-review under responsibility of The International Scientific Committee of the "14th CIRP Conference on Modeling of Machining Operations" in the person of the Conference Chair Prof. Luca Settineri

Keywords: Finite element method (FEM); Machining; Residual stress; Distortion

1. Introduction

The distortion of components is strongly related to the residual stress state induced by manufacturing processes like heat treatment, forming or machining. As simulation results show in [1], there is a significant influence of the mechanical history of a component on residual stress as a carrier of distortion potential. Higher and more heterogeneous residual stresses lead to a higher amount of distortion as [2] concluded. The correlation between increasing residual stresses and increasing amount of distortion was also observed in [3] for a grinding process. In the case of machining, material is removed forcing the component to establish a new stress equilibrium. Stresses are redistributed causing the components geometry to adjust. Especially for thin-walled components distortion potential is high. Components with a complex geometry and specific characteristics needed to fulfill their designated function are manufactured by several process steps, each affecting the initial stress state of the following process step. According to [4] the distortion potential, which is related to residual stresses, is passed on along the manufacturing process chain. Gaining knowledge about the influence of initial loads and the release of distortion for machining processes helps to increase product quality and efficiency.

2. Experimental setup

2.1. Demonstrator component

For the examination of initial loads related to the distortion potential of thin-walled components a demonstrator component has been chosen. The work

Selection and peer-review under responsibility of The International Scientific Committee of the "14th CIRP Conference on Modeling of Machining Operations" in the person of the Conference Chair Prof. Luca Settineri
doi:10.1016/j.procir.2013.06.063

piece is made of a high-strength aluminum alloy. The geometry of the demonstrator is a T-shaped component, with measures 50x50 mm base plate, 30 mm height and 5 mm thickness, see Figure 1. The specimens are manufactured from 30x50 mm bar stock of material Al 7075-T6. After cutting to cuboids with 30x50x50 mm, the T-shaped profile is generated by milling. The milling operation is done by an end mill cutter with depth of cut a_p=3 mm. During the milling operation, material is removed in several paths with the left and right side of the I-bar being machined alternately trying to avoid a tilt of the I-bar. When machining the T-profiles, as described in section 2.2, all grooves were later machined on the same side of each T-profile. Therefore, effects of up- or down-milling have been neglected, leading to comparable results.

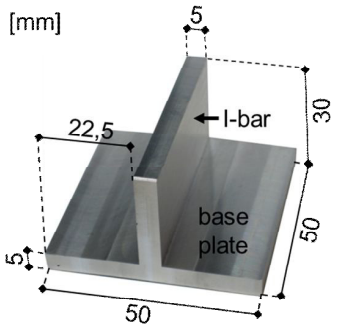

Figure 1: Geometry of the T-shaped work piece

2.2. 4-point-bending and machining

The setup for the bending operation is schematically shown in Figure 2. Different loads are applied to the T-profiles to define a variation of stress states in the component by the 4-point-bending operation. During the bending operation there is no contact between the I-bar and the bottom support. In the experiments, different forces were applied on the top support, varied in three steps with F=35, 40, 45 kN.

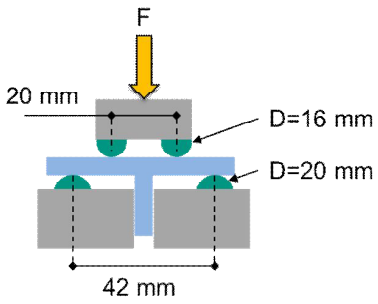

Figure 2: Scheme of 4-point-bending operation

A milling process using an end mill cutter with a diameter of 6 mm machines two different grooves into the base plate of the specimens. The grooves are realized on the right side of the component, see Figure 3. The groove geometry is varied with a depth of 2 mm and 3 mm. The I-bar of the T-profile is not machined. For the experiments, the groove is generated along the length of the base plate which is 50 mm. To ensure a good quality of the results every parameter set was carried out on three specimens and values were averaged. After both bending and machining the shape of the base plate is measured in order to evaluate the distortion released by the cutting operation.

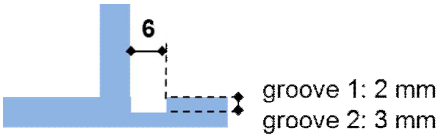

Figure 3: Machining of specimen

2.3. Measuring technique

The T-profiles are measured on a coordinate measurement machine. There are several tasks when measuring the work piece. The final work piece, a T-shaped profile, is generated by milling from a cuboid. The T-profile is then bent by applying a defined force and is machined afterwards. So for the different steps of the experiments, the measurements have to be comparable. Therefore a measurement program scans eight measurement points on each side of the cuboidal work piece and on the sides of the I-bar of the T-profile respectively in order to generate a center plane.

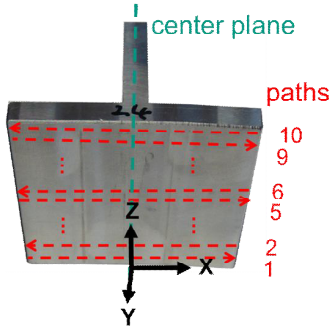

Figure 4: Measuring the specimen

With two points each measured on the top and bottom side of the work piece, the origin of the coordinate system is set, see Figure 4. This was done for the geometry of the cuboid, for the original T-profile, as well as for the bent and machined T-profile afterwards. To measure the distortion of the component, the X- and

Y-coordinates of the base plate of the T-profile are scanned along ten paths as depicted in Figure 4. For the comparison with the 2D Simulation the measured X- and Y-coordinates of paths five and six were averaged.

3. Modeling with Abaqus

3.1. Material modeling

For the work piece the material behavior of tempered aluminum alloy Al 7075-T6 is modeled using a visco-elastic-plastic behavior. Plastic hardening is defined by the Johnson and Cook plasticity model including rate dependence, describing an isotropic hardening of the work piece material. Therefore yield stress is calculated during the simulation according to the defined analytical function [5]:

$$\sigma = \left[A + B\left(\bar{\varepsilon}^{pl}\right)^{n}\right]\cdot\left[1 + C\ln\left(\frac{\dot{\bar{\varepsilon}}^{pl}}{\dot{\varepsilon}_0}\right)\right]\cdot\left(1-\hat{\Theta}^{m}\right) \qquad (1)$$

The yield stress depends on the equivalent plastic strain $\bar{\varepsilon}^{pl}$ and the temperature for including thermal-softening effects. A, B, m and n are material parameters. The nondimensional temperature $\hat{\Theta}$ is calculated with the current temperature, the reference transition temperature T_{tr} and the melting temperature T_m (all in K). The strain rate dependence is expressed by the middle term, where C is the dimensionless strain-rate hardening coefficient and $\dot{\varepsilon}_0$ is the normalizing reference strain rate. Table 1 shows the material parameters used for Johnson and Cook plasticity model, taken from [6-8].

Table 1: Material parameters

A [MPa]	546	T_m [K]	922
B [MPa]	678	T_{tr} [K]	293
C [-]	0.024	ρ [g/cm³]	2.7
m [-]	1.56	c_v [J/kg K]	896
n [-]	0.71	G [GPa]	26.5
$\dot{\varepsilon}_0$ [1/s]	1	E [GPa]	79.4

3.2. 4-point bending model

For ABAQUS/Standard version 6.11 a 2D model for 4-point bending has been built. For the bending of the T-profile two bottom supports and two top supports are used in the model assembly, shown in Figure 5. The distance between the supports and the respective diameters are analogous to the bending machine set up as prepared for the experiments, see Figure 2. The supports are modeled as rigid bodies and the work piece uses the material model described above. A concentrated force is defined as a load on the reference points of the top supports, whereas the positions of the bottom supports are fixed. The parts in the model use elements of type CPE4T with a number of elements of about 22000. There are four partitions defined in the regions where the T-profile comes into contact with the supports during the bending simulation. There, element edge size is reduced to allow proper contact generation as shown in Figure 5. In order to simulate the machining of the T-profile a defined element set was deactivated. Elements are deactivated in one pass.

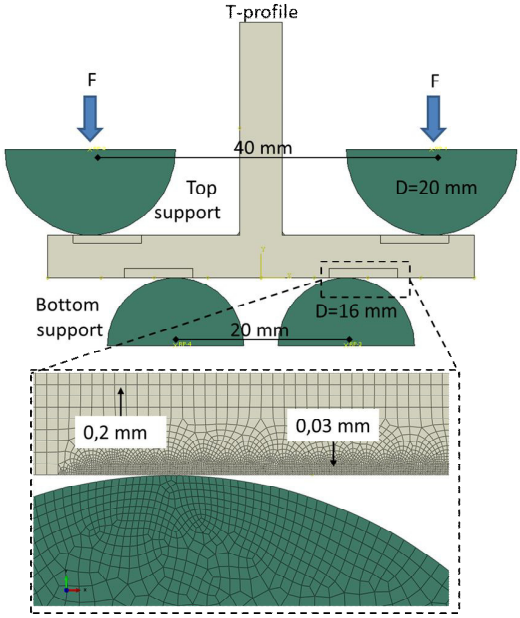

Figure 5: Assembly of the 4-point bending model

4. Results

For experimental results, Figure 6 shows an example of three T-profiles after the bending and the machining operation. For a high applied force, there seems to be a kink on the right side of the base plate which indicates that the bending operation was slightly asymmetric.

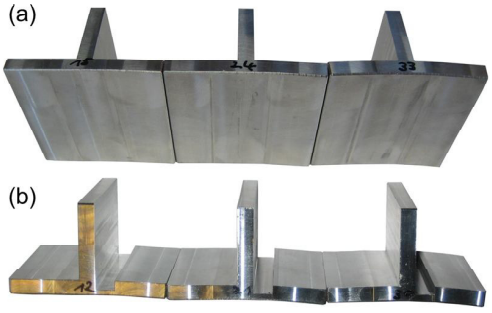

Figure 6: T-profiles applied with different loads, from left to right: F=35, 40, 45 kN, after bending (a) and after machining (b)

Simulation results in Figure 7 (a) show the residual stress state in the right half of the T-profile after it was bent with force F=35 kN and before elements have been deactivated in this area to resemble the milling of the groove. The simulated bending operations led to spacious stress fields in the base plate. In Figure 7 (b) to (d) stress profiles have been evaluated along three paths at different X-positions along the depth in Y-direction at the right side of the base plate, see Figure 7 (a). As can be seen, the stress distribution differs for the different applied forces. The higher the bending force, the higher the stress gradients in the work piece. Beneath the top surface of the base plate, a thin compressive stress field rests on a broad field of tensile stresses. In the deeper region of the work piece, going in Y-direction, a similar field of compressive stresses is followed by a thin field of tensile stresses. There is a clear influence of the bending force on the amount of tensile and compressive stresses in the midsection of the work piece between 1 and 4 mm of depth. Maximum tensile stresses increase by 40 MPa when increasing force F from 35 kN to 40 kN and by 15 MPa when increasing force F from 40 kN to 45 kN (Figure 7 (c) and (d)). For the maximum compressive stresses a similar behavior can be seen, with stresses increasing also by approximately 40 MPa and 15 MPa, respectively. Figure 7 (b) also shows a similar behavior, whereas the change in the maximum stresses is smaller. For all three profiles, the proportionality for the increasing stresses is the same when increasing the bending force. Increasing the bending force leads to a steeper stress profile in the work piece with higher gradients and a more heterogeneous stress distribution.

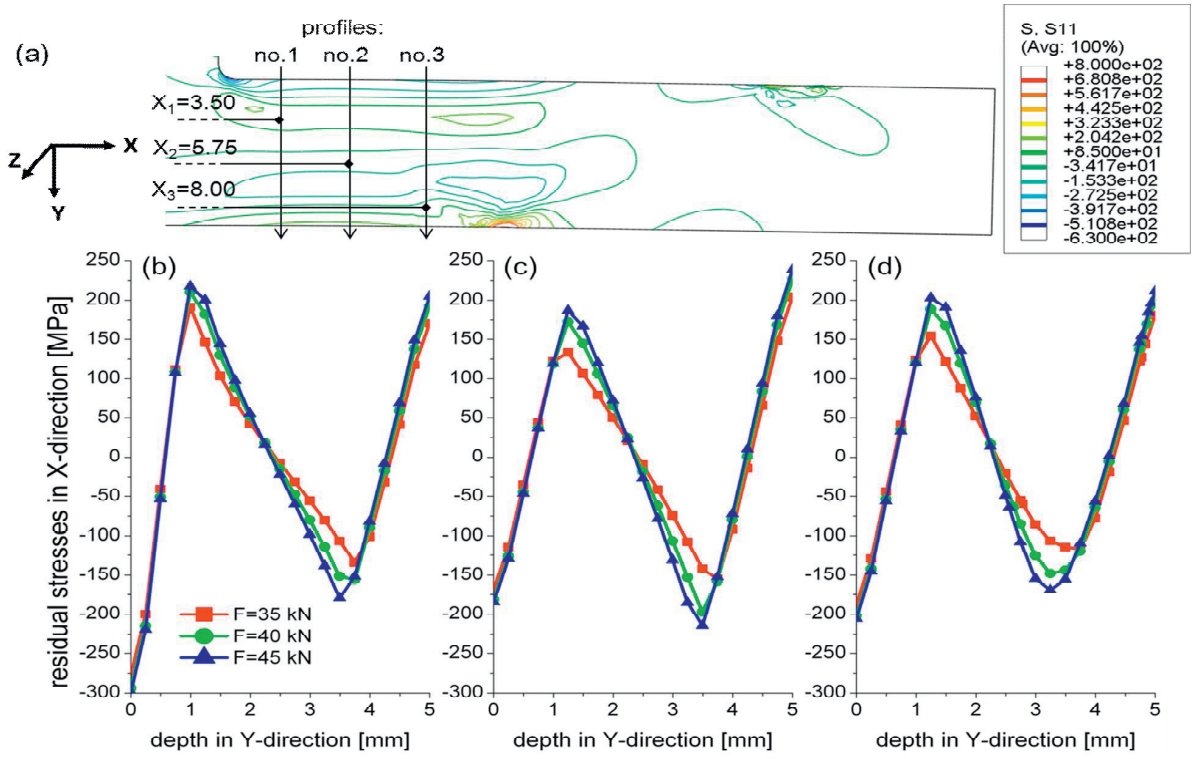

Figure 7 Residual stresses before deactivating elements, with profiles no.1 (b), no.2 (c) and no.3 (d)

In Figure 8, a comparison between numerical and experimental distortions results is shown. The amount of released distortion was evaluated, after the three different applied loads of F=35, 40, 45 kN and after a groove of 2 mm and 3 mm was machined for both simulation and experiment. Figure 8 (a) depicts numerical results of the distortion in Y-direction along the lower side of the base plate in X-direction, see also Figure 4. There clearly is an influence for a variation of the depth of the groove and the initial load on the component. For 35 kN and 2 mm groove depth the maximum distortion is -0.037 mm. An increase of the initial load to 45 kN increases the released distortion to -0.067 mm. When deactivating elements to model a groove of 3 mm depth, evaluated distortion becomes more distinctive, with the maximum distortion now ranging from -0.227 mm to -0.333 mm for forces 35 kN, 40 kN, 45 kN. Increasing the bending force increases the maximum stresses located in the components center (Figure 7, (b)-(d)). For the numerical results in Figure 8 (a), the maximum distortion for the groove of 2 and 3 mm seems to increase with the same proportionality. A

more heterogeneous stress distribution with high gradients leads to an increasing amount of distortion, as Silveira et al. stated in [2]. Figure 8 (b) shows the results from the experiments. For a machined groove with 2 mm depth, the measured distortion in the experiment is around zero. In this case, the distortion of the thin-walled components cannot be detected clearly. The values of distortion are too small and lie within the range of the machining accuracy and the repeatability of the bending operation. The influence of different loads can be evaluated clearly for a machined groove of 3 mm depth. Maximum distortion then is between -0.152 mm and -0.336 mm for forces 35 kN, 40 kN, 45 kN. For the groove of 3 mm depth the numerical and experimental results both show the same behavior of the component's distortion potential. For applied loads of F=35 kN and 40 kN the simulation model overestimates the maximum distortion by about 0.075 mm and 0.089 mm. For F=45 kN the experimental result is matched by the numerical description. As the distortion in the experiment is too small for the 2 mm groove, no comparison can be made to the simulation model.

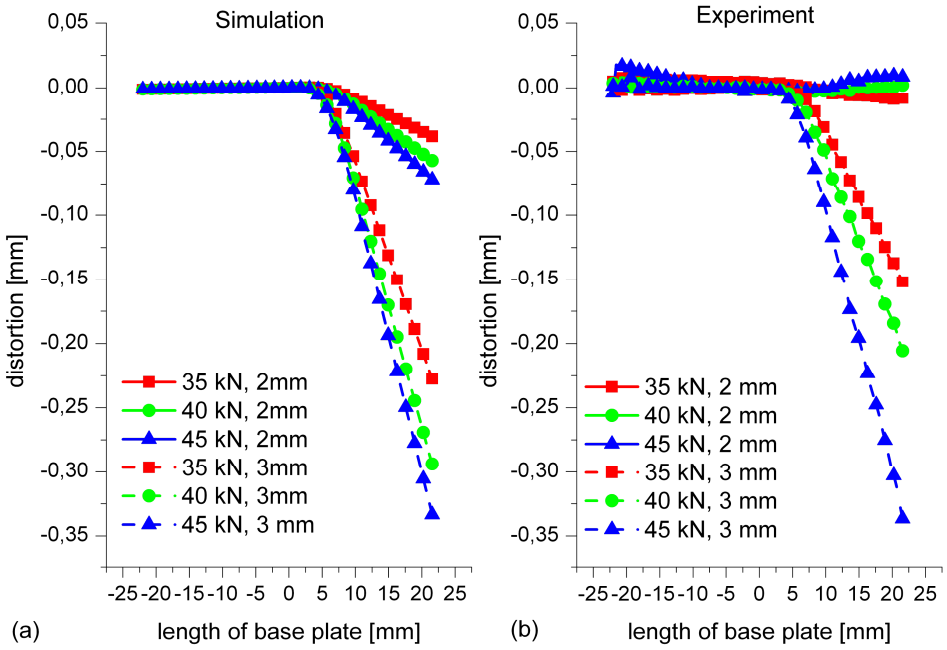

Figure 8: Numerical (a) and experimental (b) results, distortion after cutting operation

5. Conclusion and outlook

A simulation model in Abaqus has been built to investigate the distortion of a thin-walled, T-shaped demonstrator component. To define an initial stress state in the component a defined load is applied to the work piece in a 4-point-bending operation. In a numerical and experimental study a variation of loads with F=35, 40, 45 kN and two different geometries of a groove were carried out. As a result, the amount of initial stresses has a significant effect on the distortion potential, corresponding with [1]. The distortion could be quantified in the study. For the numerical results, the increase of the applied force leads to increased residual stress profiles and to an increase of released distortion of equal ratio. The simulation model describes the same behavior of the experiments. For a high load the results match very well.

For further investigations the influence of residual stresses in the semi-finished product from which the specimens are produced, the influence of different machining strategies and the influence of clamping the work piece will be studied. Also, a more realistic modeling of the machining operation, using a geometric or contact condition for the elements being removed by a rigid tool could be useful to develop a 3D model. A numerical investigation with a simulation tool which provides fast 3D capabilities is suggested.

Acknowledgements

The authors gratefully acknowledge the support of the Deutsche Forschungsgemeinschaft within the Research Training Group 1483 "Process Chains in Production: Interaction, Modeling, and Assessment of Process

Zones". The authors thank the Basque and Spanish Governments for the financial support given to the projects DESAFIO (Innpacto Program), PRO-FUTURE II (code IE11-308) and INPRORET (code IE12-342).

References

[1] Husson, R., Dantan, J.Y., Baudouin, C., Silvani, S., Scheer, T., Bigot, R., 2012. Evaluation of process causes and influences of residual stress on gear distortion. CIRP Annals - Manufacturing Technology 61, pp. 551–554

[2] Silveira, E., Irisarri, A.M., 2009. Study on the distortion of steel worm shafts. Engineering Failure Analysis 16, pp. 1090–1096

[3] Sosa, A., Echeverria, M., Moncada, O., Sikora, J., 2007. Residual stresses, distortion and surface roughness produced by grinding thin wall ductile iron plates. International Journal of Machine Tools & Manufacture 47, pp. 229–235

[4] Brinksmeier, E., Sölter, J., 2009. Prediction of shape deviations in machining. CIRP Annals – Manufacturing Technology 58, pp. 507–510

[5] Johnson, G., Cook, W., 1985. Fracture Characteristics Of Three Metals Subjected To Various Strains, Strain Rates, Temperatures And Pressures. Engineering Fracture Mechanics 23, pp. 31-48.

[6] Chen, Y., Ghosh, S., 2012. Micromechanical analysis of strain rate-dependent deformation and failure in composite microstructures under dynamic loading conditions. International Journal of Plasticity 32–33, pp. 218–247

[7] Vaziri, R., Delfosse, D., Pageau, G., Poursartip, A., 1993. High-speed impact response of particulate metal matrix composite materials – An experimental and theoretical investigation. Int. J. Impact Engng 13, 2, pp. 329-352

[8] Bae, G., Xiong, Y., Kumar, S., Kang, K., Lee, C., 2008. General aspects of interface bonding in kinetic sprayed coatings. Acta Materialia 56, pp. 4858–486